Astronomy
&
Astrophysics

X-ray flares reveal mass and angular momentum of the Galactic Center black hole

B. Aschenbach[1], N. Grosso[2], D. Porquet[1], and P. Predehl[1]

[1] Max-Planck-Institut für extraterrestrische Physik, PO Box 1312, Garching bei München 85741, Germany
[2] Laboratoire d'Astrophysique de Grenoble, Université Joseph-Fourier, BP53, 38041 Grenoble Cedex 9, France

Abstract. We have analysed the light curve of the two brightest X-ray flares from the Galactic Center black hole, one flare observed by *XMM-Newton* on October 3, 2002 (Porquet et al. 2003), and the other flare observed by *Chandra* on October 26, 2000 (Baganoff et al. 2001). The power density spectra show five distinct peaks at periods of ~100 s, 219 s, 700 s, 1150 s, and 2250 s common to both observations within their estimated measurement uncertainties. The power density spectrum of the recently reported infrared flare of June 16, 2003 (Genzel et al. 2003) shows distinct peaks at two, if not three, periods (including the 1008 ± 120 s infrared period), which are consistent with the X-ray periods. The remaining two periods could not be covered by the infrared measurements. Each period can be identified with one of the characteristic gravitational cyclic modes associated with accretion disks, i.e. either Lense-Thirring precession, Kepler orbital motion and the vertical and radial epicyclic oscillation modes, in such a way that a consistent value for the black hole mass of $M_{\rm BH} = 2.72^{+0.12}_{-0.19} \times 10^6 \ M_\odot$ and the angular momentum $a = 0.9939^{+0.0026}_{-0.0074}$ is obtained. The available data on $M_{\rm BH}$ derived from studies of the orbital motion of the S2 (S0-2) star (Schödel et al. 2002; Ghez et al. 2003) agree with our findings. Finally we discuss some implications of the fairly high value for the angular momentum.

Key words. Galaxy: center – X-rays: individuals: Sgr A* – radiation mechanisms: general – relativity – Galaxy: nucleus – Galaxy: fundamental parameters

1. Introduction

The region towards the Galactic Center (GC) has been recently resolved in X-rays by *Chandra* measurements (Muno et al. 2003; Baganoff et al. 2003). A source was identified as X-ray counterpart of the GC black hole Sgr A*. The quiescent X-ray luminosity turns out to be extraordinary low $(2.2 \times 10^{33} \ {\rm erg \, s^{-1}}$, Baganoff et al. 2003) for a mass accreting black hole, given its mass which has been measured through the motion of the S0-2 star orbiting the black hole. Mass values range from $2.2 \times 10^6 \ M_\odot$ (lower limit of Schödel et al. 2002), $3.6 \times 10^6 \ M_\odot$ (Genzel et al. 2003) to $4.1 \pm 0.6 \times 10^6 \ M_\odot$ for a distance of 8 kpc (Ghez et al. 2003). Various models to explain the low luminosity have been proposed and discussed quite controversially including low accretion rates and radiatively inefficient accretion flows, for example. For a brief overview see for instance Melia & Falcke (2001), Baganoff et al. (2001), Porquet et al. (2003) and Yuan et al. (2003). The quiescent state is interrupted by occasional, sometimes very bright, flares. The first bright flare with a peak luminosity of $1 \times 10^{35} \ {\rm erg \, s^{-1}}$ (Baganoff et al. 2001) was observed with the *Chandra* ACIS-I instrument on October 26, 2000. An even brighter X-ray flare with a peak luminosity of $3.6 \times 10^{35} \ {\rm erg \, s^{-1}}$ occurred on October 3, 2002 and was caught with the *XMM-Newton* EPIC instruments (Porquet et al. 2003). It is generally accepted that the radiation is from or at least channeled through the accretion disk orbiting the central black hole. Some models for the creation of flares have been brought forward, e.g., Markoff et al. (2001) suggest extra electron heating near the black hole, Liu & Melia (2002) propose a sudden enhancement of accretion and Nayakshin & Sunyaev (2003) prefer stars passing the disk. We think that the high luminosity involved in the flares suggests that somehow the inner regions of the accretion disk play a major role, basically because of the increased gravitational potential. Sporadic events like flares are then likely to take us closer to the black hole and enable us to discover more easily periodic or quasi-periodic changes in the light curve of a flare, like the Kepler frequency of the innermost marginally stable orbit, and others, by which mass and angular momentum of the central black hole could be determined. That this idea might have some bearing has been recently demonstrated by the discovery of a 16.8 ± 2 min period in two infrared flares (Genzel et al. 2003). Genzel et al. tentatively assign the period to the length of the marginally stable orbit and, adopting a mass of $3.6 \times 10^6 \ M_\odot$, they calculate an angular momentum of $a = 0.5$ for the black hole.
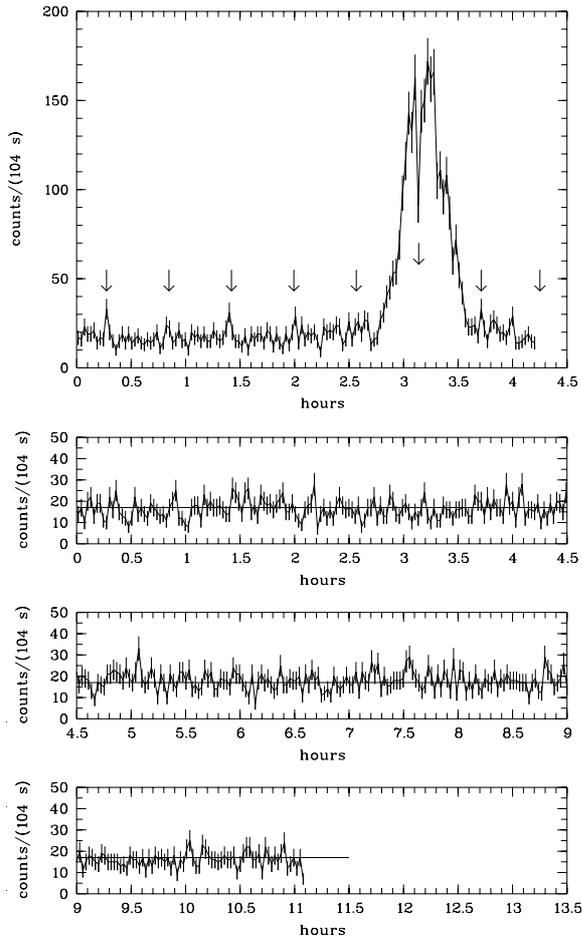
Fig. 1. EPIC light curves (MOS 1+MOS 2+PN) of the *XMM-Newton* observation of October 3, 2002 (*upper panel*, Fig. 1a) and the February 26, 2002 observation (*lower three panels*, Fig. 1b). Error bars indicate 1σ uncertainties. The horizontal line in the lower three panels corresponds to the mean count rate level. Arrows mark peaks associated with a 2178 s periodic signal.

Fig. 2. ACIS-I light curves of the *Chandra* observation of October 26, 2000 (*upper panel*, Fig. 2a) and the May 25, 2002 observation (*lower three panels*, Fig. 2b). Error bars indicate 1σ uncertainties.

In Sect. 2 we show the light curves of the two brightest X-flares, which we have analysed including but separated from the time sections before and after the flare proper, as well as two very long (11 h and 46 h) X-ray light curves representing the so-called quiescent state. Like the two flares one event was observed by *XMM-Newton* and the other event was covered by *Chandra*. These two observations were primarily analysed for cross-checking with the flare characteristics. Section 2 also contains the power density spectra (PDS) of the relevant light curves. Five groups of characteristic frequencies with at least two detections per group have been found. In Sect. 3 we describe the relation of these periods with the cyclic gravitational modes thought to be possibly created in accretion disks, i.e. the Lense-Thirring precession frequency, the Kepler frequency and the vertical and radial epicyclic frequencies. In Sect. 3 we also describe how we derive the values for M_{BH} and the angular momentum a (the Kerr parameter) from the frequencies measured. We include in our analysis the power density spectra of the two infrared flares published by Genzel et al. (2003). Finally we
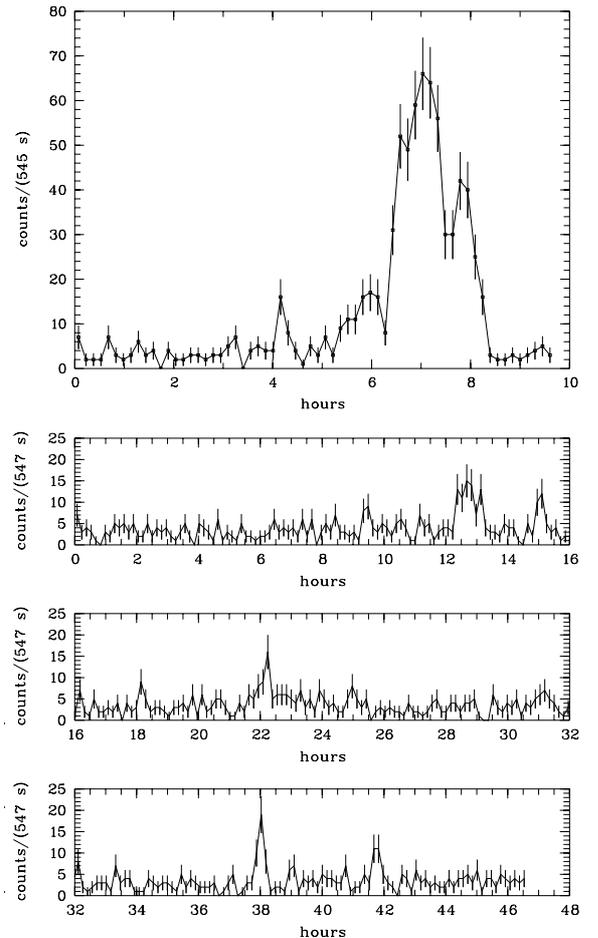
discuss a few implications which result from the fairly high value of a we have obtained.

2. Observations and analysis

2.1. Light curves

Figure 1a shows the light curve of the October 3, 2002 flare observed by *XMM-Newton* and published by Porquet et al. (2003) with a slightly different time binning. Figure 1b shows the light curve of an ~11 h quiescent period obtained by *XMM-Newton* on February 26, 2002. Figure 2a displays the light curve of the very first flare reported from Sgr A* dated October 26, 2000, observed with *Chandra* and published by Baganoff et al. (2001). We choose a slightly different energy band and a different binning. Sgr A* was observed for 46.5 h on May 5/6, 2002 without a bright flare occurring, and the *Chandra* light curve is shown in Fig. 2b. Because of the numerous peaks the source is apparently not in a true quiescent state but exhibits quite a number of smaller flux increases or small flares. The essential observational details are summarized in Table 1. The *XMM-Newton* data have been proprietary PI data, which by now are publicly available. The *Chandra* data have

Table 1. Summary of observations analysed (cf. Figs. 1 and 2). Instr. I is EPIC PN+MOS1+MOS2 on *XMM-Newton*, and instr. II is ACIS-I on *Chandra*. Date is in day/month/year.

Instr.	Observ. date	Total time (min)	Flare time (min)	Preced. time (min)	Sampl. time (s)
I	03/10/02	254.1	56.33	197.8	2.6
I	26/02/02	667.2	–	–	2.6
II	26/10/00	589.3	115.3	372.4	3.241
II	25/05/02	2804.2	–	–	3.141

been extracted from the public *Chandra* archive (level 2 processed event list, provided by the *Chandra X-ray Center*). We restrict our analyses to just these four data sets because they cover the two brightest flares and the other two observations have the longest exposure of the so-called quiescent state. For the timing analysis we added PN, MOS1 and MOS2 data in one set using counts, which were for *XMM-Newton* extracted from a circle of $10''$ radius with energies between $2.6-10$ keV. For the *Chandra* data the extraction radius was $1.5''$ around the archived source position, and the energy band is $2.0-8$ keV.

Because of the relatively broad point spread function of *XMM-Newton* the extraction radius of $10''$ contains emission from more objects than just Sgr A*. The *Chandra* image reveals another four or five additional sources as well as diffuse emission. Baganoff et al. (2003) estimate a net count rate of $5.74 \pm 0.40 \times 10^{-3}$ count s^{-1} for Sgr A* in its quiescent state. The power law spectrum has a photon index of $\Gamma_q = 2.7^{+1.3}_{-0.9}$ and an absorbing column density $N_{H,q} = 9.8^{+4.4}_{-3.0} \times 10^{22}$ cm^{-2}. Using the best fit values we estimate a Sgr A* quiescent state count rate of 0.029 ± 0.003 count s^{-1} for MOS 1+MOS 2+PN, so that the conversion factor is 5 ± 0.5 between the two instrument combinations. The mean EPIC count rate of Sgr A* in its quiescent state amounts to 0.16 count s^{-1} (cf. Fig. 1b), which means that the background sources are likely to contribute on average 0.013 count s^{-1} or 82% of the total during the Sgr A* quiescent state, provided that neither the background sources nor Sgr A* have changed significantly compared to the October 26, 2000 observation. When we subtract the count rate of the background from the flare observation (Fig. 1a) the peak count rate during the time preceding the actual flare has a level of 0.125 ± 0.03 count s^{-1}, which means that the precursor section is ~ 4 times brighter than Sgr A* in its quiescent state. It is interesting that flares observed in the infrared by Genzel et al. (2003) show about the same ratio of the flare peak intensity and the quiescent level. This suggests that the X-ray precursor and the infrared flares originated in the same process and that, given the huge X-ray flares, much brighter infrared flares still await their detections.

Conversion of instrument count rates to flux density requires knowledge of the source spectrum and column density of the photoelectrical absorption. This is available for the quiescent state measured by *Chandra* (Baganoff et al. 2003), the October 26, 2000 flare measured by *Chandra*
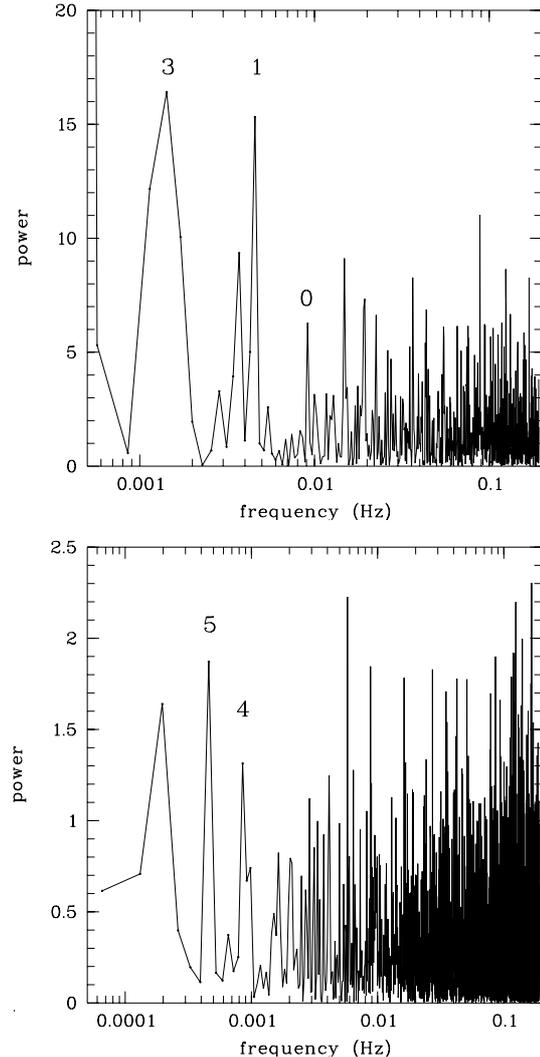

Fig. 3. Power density spectra of the October 3, 2002 flare (*upper panel*, Fig. 3a) and its precursor section (*lower panel*, Fig. 3b); *XMM-Newton* measurement.

(Baganoff et al. 2001) and the October 3, 2002 flare measured by *XMM-Newton* (Porquet et al. 2003). Since both the spectrum and the absorption column density differ among the three observations we provide conversion factors for the EPIC count rate and the ACIS-I count rate for each of the three states. These are: 9.5 μJy (EPIC counts/s)$^{-1}$, 47.6 μJy (ACIS-I counts/s)$^{-1}$ (quiescent); $0.5^{+1.1}_{-0.3}$ μJy (EPIC counts/s)$^{-1}$, $2.8^{+6.1}_{-2.0}$ μJy (ACIS-I counts/s)$^{-1}$ (*Chandra* flare); 12.3 μJy (EPIC counts/s)$^{-1}$, 71.8 μJy (ACIS-I counts/s)$^{-1}$ (*XMM-Newton* flare). The relatively large uncertainty of the conversion factor for the *Chandra* flare are due to the uncertain spectrum and column density. The energy flux densities are given for $E = 1$ keV.

2.2. Power spectra

From the light curves shown in Figs. 1 and 2, power density spectra (PDS) have been created by a Fourier analysis of six data sets. Two sets cover the time section of just the flare, one each for *XMM-Newton* (Fig. 3a) and *Chandra* (Fig. 4a); another two sets cover the time sections before
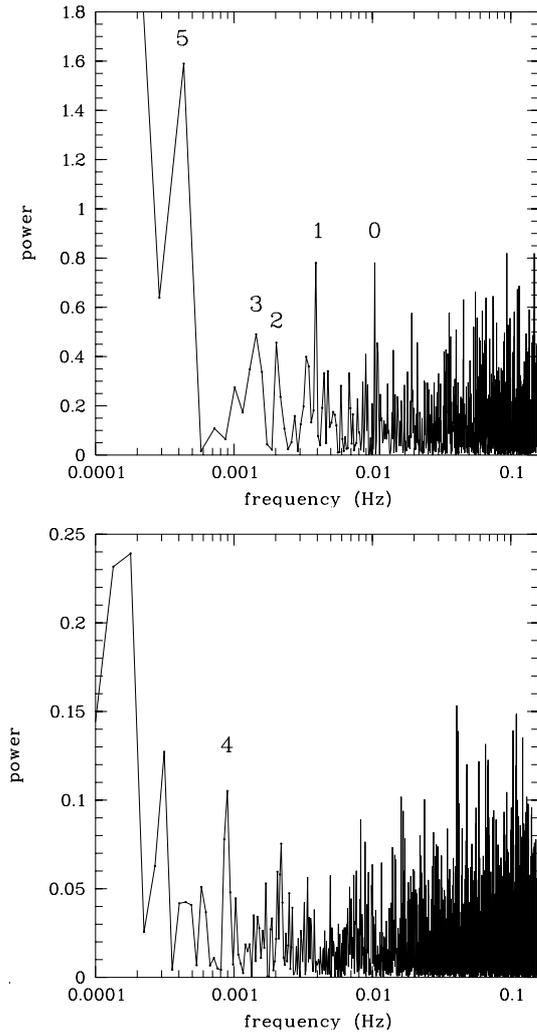
Fig. 4. Power density spectrum of the October 26, 2000 flare (*upper panel*, Fig. 4a) and its precursor section (*lower panel*, Fig. 4b); *Chandra* measurement.
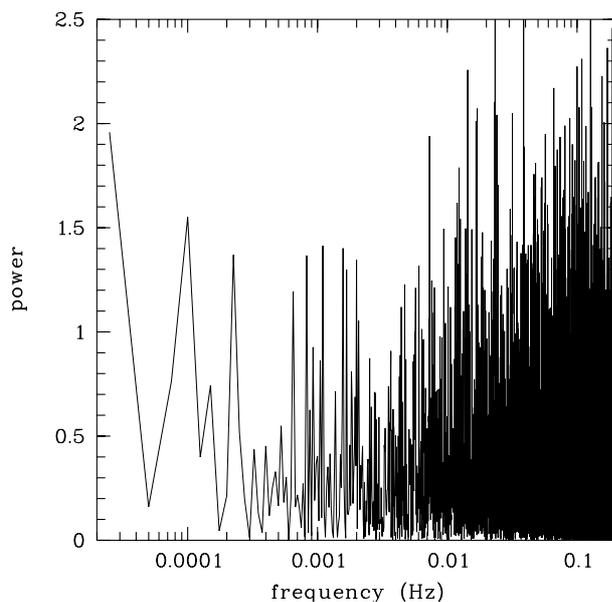

Fig. 5. Power density spectrum of the February 26, 2002 quiescent state; *XMM-Newton* measurement.
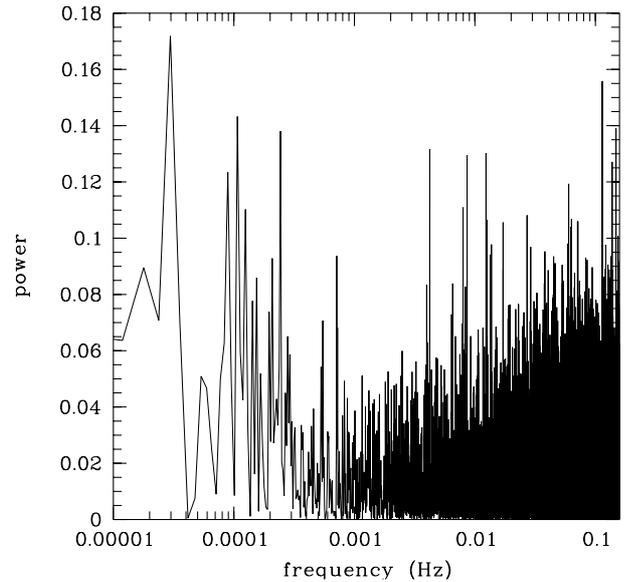

Fig. 6. Power density spectrum of the May 25, 2002 quiescent state; *Chandra* measurement.

and after the flare (Figs. 3b and 4b). For these PDS the data of the flare proper have been removed and replaced by data with a mean flux identical to that of the time preceding the flare assuming a Poissonian statistical distribution. The final two sets correspond to the two observations of the quiescent level (Figs. 5 and 6). We define the power spectral density psd_n at a frequency f_n and wave number n as $psd_n = (a_n^2 + b_n^2)/(2 \times \Delta t^2) \times T$; a_n and b_n are the Fourier coefficients, Δt is the sampling or binning time and T is the total observing time (Table 1). The Fourier coefficients are in units of ACIS-I counts^{-1} for the *Chandra* observations and EPIC counts^{-1} for the *XMM-Newton* observations. Because of the different efficiencies the psd_n's are expected to generally differ by a factor of $\sim 25 \pm 5$ for the same luminosity level given the energy spectrum described in Sect. 2.1.

2.3. Frequencies

In general the six PDS look very much alike. There is a high frequency component which is more or less rapidly growing with increasing frequency, which reflects the noise introduced by the low counting statistics. We note that the smallest possible binning has been chosen so that we deal with just no or one count per bin. At low frequencies the PDS are dominated by a few high peaks, which summarize the mean shape of the light curves, averaged over periods which are just a few times shorter than the whole track. Clearly separated from these two regimes is a low noise mid-frequency section between ~ 0.7 mHz and ~ 7 mHz for the flare observations (Figs. 3a and 4a), and 0.7 mHz and 2.5 mHz for the flare precursor sections (Figs. 3b and 4b). In this frequency band we see two distinct PDS peaks at 1.426 mHz and 4.562 mHz (Fig. 3a; labels 3 and 1, respectively; *XMM-Newton* flare) and similarly at 1.445 mHz and at 3.902 mHz (Fig. 4a; labels 3 and 1, respectively; *Chandra* flare), standing well above the noise level

in the corresponding frequency bands. In the *Chandra* flare we see a third peak at 10.41 mHz (label 0), which, however, is located at the beginning of the climbing high frequency noise section (Fig. 4a). The *XMM-Newton* flare PDS shows a similar close-by peak at 9.12 mHz (label 0), although at a fairly low power level. Like in the *Chandra* case this frequency is at the high frequency edge of the low-noise band. The existence of this pair of frequencies might be doubtful but they should be noted basically because they seem to appear in two different observations. These are the only pairs in the flare section. Absent in the *XMM-Newton* PDS but fairly prominent in the *Chandra* PDS (Fig. 4a) is a peak at ~2 mHz (label 2).

The PDS of the data preceding the flare also show distinct peaks in the low noise regime at 0.853 mHz (Fig. 3b, label 4; *XMM-Newton*) and 0.895 mHz (Fig. 4b, label 4; *Chandra*); a further peak appears in the *XMM-Newton* PDS at 0.459 mHz (label 5). The power at this frequency is so high that the equivalent period of 2178 s can be identified by peaks in the light curve (cf. arrows in Fig. 1a). A PDS peak associated with or close to 0.459 mHz is clearly absent in the *Chandra* flare precursor observation but there is a peak at 0.434 mHz in the *Chandra* flare (label 5).

The PDS is a function of discrete frequencies given by $f_n = \frac{n}{T}$ with $1 \leq n \leq \text{int}(\frac{T}{2\,\Delta t})$ and Δt the binning size. Therefore, there is in principle a systematic relative frequency uncertainty possible of $(\frac{\Delta f}{f})_n = \pm(\frac{1}{n-1})$. In Table 2, we summarize the results including frequency f, wave number n, period P, power spectral density *psd* and a label ID, which has the same value for frequencies close to each other. The same ID's are shown as labels in the PDS graphs. We find in the *XMM-Newton* and the *Chandra* observations five groups of periods, each of which is a pair with one member from *XMM-Newton* and one from *Chandra*. The periods of the members of each pair are almost identical, i.e. 110/96 s (label 0), 219/256 s (1), 701/692 s (3), 1173/1117 s (4), 2178/2307 s (5). They appear to be not exactly identical but conceding the maximal possible uncertainty they are consistent with each other. This coincidence strongly supports their existence and suggests that each pair represents the same process.

Genzel et al. (2003) have published the discovery of a 16.8 ± 2 min period in the two infrared flares observed on June 15 and June 16, 2003. A look at the two published PDS shows that there are more peaks, which we have read off from their Fig. 2c and added to Table 2 (IR/15, IR/16). Except the peak at 321 s and wave number $n = 16$, appearing in the June 16 flare, each frequency has a close-by counterpart in the *XMM-Newton* and/or *Chandra* PDS adding another finding to groups 1, 2, 3 and 4. Of course, the *psd* at 214 s in IR/16 is fairly low but it shows up as a local maximum. There is no peak at the frequencies of group 5 in the infrared observations, which however have been too short to search for it. Obviously, the infrared frequencies are fully consistent with the X-ray frequencies.

We note that at none of the frequencies selected from the flares or precursors a prominent *psd* is evident in the quiescent level observations. The PDS of the quiescent level observations are shown in Fig. 5 (*XMM-Newton*) and Fig. 6 (*Chandra*). The *XMM-Newton* PDS shows a set of six prominent PDS peaks between 0.65 mHz and ~2 mHz centered on ~1 mHz.

Table 2. Compilation of outstanding frequencies. [1] The *psd* is given in units of $(\text{count s}^{-1})^2\,\text{Hz}^{-1}$. For *XMM EPIC* count rates and for *Chandra* ACIS-I, count rates are quoted. na: not applicable, i.e., not covered because the flare didn't last long enough. The lower section of the table contains the frequencies of high *psd* observed in the two infrared flares by Genzel et al. (2003). The data have been read off their Fig. 2c.

State/ Instrum.	f (mHz)	n	P (s)	*psd* [1]	ID
Flare					
XMM	9.123	32	110	6.3	0
Chandra	10.41	72	96	0.78	0
XMM	4.562	16	219	15.3	1
Chandra	3.902	27	256	0.78	1
XMM	–	–	–	–	–
Chandra	2.023	14	494	0.46	2
XMM	1.426	5	701	16.4	3
Chandra	1.445	10	692	0.49	3
XMM	na	na	na	na	na
Chandra	0.434	3	2307	1.6	5
Precursor					
XMM	0.853	13	1173	1.3	4
Chandra	0.895	20	1117	0.11	4
XMM	0.459	7	2178	1.9	5
Chandra	–	–	–	–	–
IR flare					
IR/16	4.76	24	214	–	1
IR/15	2.0	6	498	–	2
IR/16	1.39	7	733	–	3
IR/15	1.0	5	996	–	4
IR/16	0.99	5	1026	–	4

This frequency band embraces the 0.853/0.895 mHz peaks of both the *XMM-Newton* and *Chandra* flare precursors. The *psd*'s at the six frequencies vary between 1.05 and 1.42 (EPIC count $\text{s}^{-1})^2\,\text{Hz}^{-1}$ which is close to what is observed as power for the 1173 s period for the flare precursor (Table 2). A *psd* peak at the period of 2178 s is not present in the quiescent observations. The PDS of the *Chandra* quiescent level observations doesn't show prominent peaks around one mHz (Fig. 6). But extrapolating the *XMM-Newton psd* of ~1.2 (EPIC count $\text{s}^{-1})^2\,\text{Hz}^{-1}$ the equivalent *Chandra psd* is expected to be close to the noise level.

The lowest frequencies accessible for this investigation are covered by the *Chandra* May 25, 2002 observation, with no bright flare though (Fig. 6). Starting at ~0.1 mHz the *psd* drops rapidly with frequency reaching the noise level minimum at ~0.4 mHz. The region between 0.18 mHz and 0.35 mHz

seems to show excess power peaking at ~0.24 mHz or 4100 s. In this band the *XMM-Newton* PDS is very similar to the *Chandra* PDS with fairly high peaks at 0.225 mHz and 0.1 mHz, but details like in the *Chandra* observation are not resolved because of the shorter exposure (Fig. 5). This *psd* structure is probably not related to the occurrence rate of flares, which has been estimated to 1.2 ± 0.6 per day by Baganoff (2003), which is a factor of about 17 lower in frequency. Excluding the 0.18 mHz−0.35 mHz band the PDS, with 20 single *psd* values remaining, can be fitted by a power law with an index of roughly −2.3. We stress that the statistics are poor and we don't claim the existence of a QPO but the excess between 0.18 mHz and 0.35 mHz looks like a QPO structure. QPO's (quasi-periodic oscillations), which show up as a band of increased *psd* above an underlying, much broader PDS, which has the shape of a power law, have been observed in a number of galactic binaries, containing a compact object like a neutron star or black hole. The QPO's are considered to be created in associated accretion disks (e.g., van der Klis 2000). As Nowak & Lehr (1998) and others have pointed out, QPOs arising from supermassive black holes in AGN are expected to show periods between three hours and years, if a 0.1 s period is typical for a galactic black hole and if periods scale with mass. Such long periods are very difficult to measure for current missions. But for the Galactic Center black hole with its fairly low mass QPO periods might be shorter. In fact, if we scale the 300 Hz, which is the highest QPO frequency observed in the 7 $M_\odot$ black hole microquasar GRO J1655−40 (Remillard et al. 1999; Orosz & Bailyn 1997) we expect a QPO around 0.6 mHz for the Galactic Center black hole, which is well within the long duration *Chandra* and *XMM-Newton* measurements.

2.4. Statistical significance

To quantify the significance of a measured *psd* value we have approximated the rather erratic flare light curves by some smooth functions which reproduce very well the general shape but do not introduce high frequency variations in the regime which contains the frequencies to be investigated. We are particularly interested in the frequencies of group 0 and group 1. The lower frequencies may be too much biased by red noise for which we don't have a model. The model light curve of the *XMM-Newton* flare consists of three exponentials, one for the rise, one for the top and the third for the decay. The model light curve for the *Chandra* flare is set up by a four piece polygon. Each model light curve is normalized to the total number of measured counts. The model light curves are binned with the same sampling time as the measured data, and the model counts per bin are subject to Poissonian statistics. For each flare $Z = 3 \times 10^5$ light curves have been produced, Fourier analysed and the PDS calculated.

The significance of a power peak is defined via a confidence level S, which gives the probability that the detected power $psd_{n,\text{detect}}$ is not produced by the noise process, i.e. $1 - S = N_{\text{trials}} \times W(psd_n \geq psd_{n,\text{detect}})$ (van der Klis 1989). W is the ratio of the number of powers exceeding $psd_{n,\text{detect}}$ and Z. N_{trials} is the number of frequencies for which the PDS has been

measured, which is 674 and 1066 for the *XMM-Newton* and *Chandra* flare, respectively. We stress that we have not made use of a fixed form for W like a χ^2 or Gaussian distribution, but we built W by Monte Carlo simulations (cf. van der Klis 1989). The simulations show that there are some significant peaks, i.e. for group 0: $S(96\ \text{s}) = 0.989$ whereas the *psd* at 110 s of the *XMM-Newton* flare is consistent with a noise created peak; for group 1: $S(219\ \text{s}) = 0.993$ and $S(256\ \text{s}) = 0.947$, which means that signals with the latter periods quite likely exist. There is just one more pair of close-by frequencies each of which shows a significant *psd*, which are at a period of 11.31 s with $S(11.31\ \text{s}) = 0.634$ in the *XMM-Newton* flare and of 10.68 s with $S(10.68\ \text{s}) = 0.968$ in the *Chandra* flare. This very short period should be kept in mind for future studies.

We also tried quite a few different model light curves but they do not change significantly the values for S given before.

3. Discussion

Five characteristic frequency groups have been discovered in the X-ray flares with their existence being supported by the fact that they have been found in more than one observation. We try to identify each of these frequencies with one of the oscillation modes which could occur in accretion disks surrounding black holes. As Nowak & Lehr (1998) for instance point out there are four cyclic modes which could give rise to periodic or quasi-periodic changes in accretion disks. These modes are based on gravitation but it is an open question whether they would create changes of the light output at the very same frequencies. However, Nowak & Lehr (1998) point out that the mode frequencies predominantly depend upon fundamental gravitational frequencies and are not strongly affected by hydrodynamic processes for thin disks.

3.1. Characteristic accretion disk frequencies

There are four cyclic gravitational modes associated with black hole accretion disks (Nowak & Lehr 1998, Eqs. (1) to (3); Merloni et al. 1999, Eq. (4)), which are the Kepler frequency (Ω_K), the disk perturbation frequencies in vertical and radial direction called vertical (Ω_V) and radial (Ω_R) epicyclic frequency and the Lense-Thirring precession frequency (Ω_{LT}). Each frequency depends on the central mass M, the angular momentum a and the radial distance r from the center. Equations (1) to (4) show the relations, for which the standard notation of $c = G = 1$ is used. Physical length scales are in units of GM/c^2 and angular frequencies Ω are in units of c^3/GM. $r = 1$ is defined as the gravitational radius r_g.

$$\Omega_K = (r^{3/2} + a)^{-1} \tag{1}$$

$$\Omega_V^2 = \Omega_K^2 \left(1 - \frac{4a}{r^{3/2}} + \frac{3a^2}{r^2}\right) \tag{2}$$

$$\Omega_R^2 = \Omega_K^2 \left(1 - \frac{6}{r} + \frac{8a}{r^{3/2}} - \frac{3a^2}{r^2}\right) \tag{3}$$

$$\Omega_{LT} = \Omega_K - \Omega_V. \tag{4}$$

3.2. Arrangement of frequencies and modes

Equations (1) to (4) show that Ω_K decreases monotonically with increasing r and, on the contrary, for a fixed, both Ω_V and Ω_R initially rise with r, go through a maximum and then decrease with increasing r. Ω_V reaches its maximum at a radial distance denoted by $r = r_{V\max}$ and Ω_R takes its maximum value at a distance denoted by $r = r_{R\max}$. For any r and a fixed $\Omega_K \geq \Omega_V > \Omega_R$. This means that the shortest period is to be assigned to Ω_K at the smallest r possible which is the innermost marginally stable orbit at $r = r_{ms}$ defined by $\Omega_R = 0$. For each of the other frequencies there is a choice between $\Omega_V(r = r_{ms})$, $\Omega_V(r = r_{V\max})$, $\Omega_V(r = r_{R\max})$, $\Omega_R(r = r_{V\max})$ and $\Omega_R(r = r_{R\max})$. $\Omega_R(r = r_{ms})$ is excluded because $\Omega_R(r = r_{ms}) = 0$ per definition. Whether Ω_{LT} could be generated at $r > r_{ms}$ is hard to tell, but $\Omega_{LT}(r = r_{ms})$ could approach $\Omega_K(r = r_{ms})$ or could even be lower than the frequency of any other mode, depending on a. We have chosen three radial fix points, i.e. $r = r_{ms}$, $r = r_{V\max}$ and $r = r_{R\max}$. In principle there is no preference for any r except for $r = r_{ms}$ but we note that Ω_V and Ω_R do not vary a great deal with r over a reasonable range of r centered on $r_{V\max}$ or $r_{R\max}$, respectively. In the following we use periods, i.e. P_{LT}, P_K, P_V and P_R instead of angular frequencies Ω. Each observed period is now assigned to one mode at either r_{ms}, $r_{V\max}$ or $r_{R\max}$ each resulting in a relation between M_{BH} and a. If these assignments cover all observed periods within their measurement uncertainties, a common value of M_{BH} and a should emerge. Group 0 contains the shortest period of 110 s; if assigned to $P_K(r = r_{ms})$ an upper limit for $M_{BH} < 1.78 \times 10^6\ M_\odot$ exists for $a \to 1$, which is in conflict with the lowest value of $2.2 \times 10^6\ M_\odot$ published by Schödel et al. (2002). Therefore this ascription is excluded. The next longer period of 219 s implies an upper limit of $M_{BH} < 3.55 \times 10^6\ M_\odot$ if assigned to $P_K(r = r_{ms})$. This is within the range of values for M_{BH} reported in the literature and suggests the assignment to Keplerian motion along the marginally stable orbit.

The only solution of Eqs. (1) to (4) with consistent values for M_{BH} and a is obtained for the following assignation of period and mode:
group 1, 219 s $= P_K(r = r_{ms})$ [K];
group 3, 692 s $= P_V(r = r_{ms})$ [V];
group 4, 1117 s $= P_R(r = r_{R\max})$ [R].
With this set Eq. (4) predicts $P_{LT} \approx 320$ s. Such a period shows up with increased power in the June 16 infrared flare (321 s, Genzel et al. 2003, cf. Sect. 2.3). The four relations for M_{BH} versus $(1 - a)$ following from Eqs. (1) to (4) are drawn in Fig. 7, which shows an almost perfect, single intersection of the four relations. The wide error polygon of Fig. 7 indicates the maximal range for M_{BH} and $(1 - a)$ without the 321 s period and the inner polygon covers the constraints set by the 321 s period. This solution does not suggest a specific radius like r_{ms}, $r_{V\max}$ or $r_{R\max}$ for the remaining period of ∼500 s, but it is consistent with a Kepler period expected close to $r = r_{R\max}$. The periods of group 5 around 2200–2300 s, cannot arise from a region $r < r_{R\max}$. However, we point out that this period is very close to just twice the period of the radial epicyclic mode and might indicate a dominance of the amplitude of every second
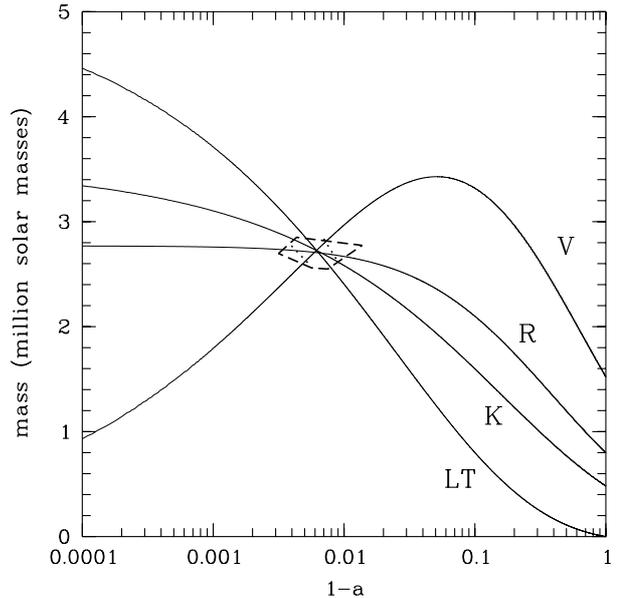

Fig. 7. Relation of M_{BH} versus $(1 - a)$. Each curve represents one period assigned to a specific gravitational mode, coded by a label described in the text. The error region is enclosed by the dashed polygon. The dotted polygon is narrower because of the additional constraints imposed by the 321 s period (LT).

cycle. We note that the group 0 period of ∼100 s is close to the first harmonic ($m = 2$) expected for the "diskoseismology" C-mode (Nowak & Lehr 1998).

The best-fit solution to the intersections is $M_{BH} = 2.72^{+0.12}_{-0.19} \times 10^6\ M_\odot$ and $a = 0.9939^{+0.0026}_{-0.0074}$. The errors quoted are not 1σ errors but reflect the maximal possible uncertainty given by the maximal uncertainties of the period determination. The radii involved are $r_{ms} = 1.371$ and $r_{R\max} = 2.507$. The gravitational radius ($r = 1$) amounts to 4.1×10^{11} cm.

Independent measurements of the orbital motion of the star S0-2 (S2) around the GC black hole have resulted in $M_{BH} = 3.7 \pm 1.5 \times 10^6\ M_\odot$ (Schödel et al. 2002) and $M_{BH} = 4.07 \pm 0.62 \times 10^6\ M_\odot$ $(R_0/8\ \mathrm{kpc})^3$ (Ghez et al. 2003) with R_0 the distance to the black hole. Our result is consistent with the Schödel et al. measurement at their $1\ \sigma$ level and it also agrees with Ghez et al.'s measurement at their 2σ level and $R_0 = 8$ kpc. Earlier Genzel et al. (1996) determined M_{BH} to 2.5–3.0 $\times 10^6\ M_\odot$ from measurements of dark matter concentration in the central parsec of the Milky Way which appears to match our result best.

3.3. The high value of a

The high value of $a \approx 1$ means that the emission from the inner parts of the accretion disk is quite close to the black hole. The event horizon is located at $r_H = 1.112$. With $r_{ms} = 1.371$ the distance to the marginally stable orbit is just 3.6 light seconds. Light from matter crossing the marginally stable orbit is therefore very likely to disappear in a fairly short time. Is the PDS peak at ∼11 s the characteristic time scale at which the light is fading away? The light curve of the *XMM-Newton* flare (Fig. 1a) shows a deep, very short (<100 s) cut close to

maximum light, which might be such an event. A similar event is also seen in the *Chandra* flare (Fig. 2a). The arrows plotted in Fig. 1a point to the maxima of the 2178 s period, which seem somehow to synchronize with the deep cut in the light curve. According to our arrangement scheme the 2178 s period is characteristic for the radial epicyclic mode and it looks as if matter is pushed across the marginally stable orbit.

The high value of $a \approx 1$ and the proximity of the inner region to the event horizon also implies that fairly low (<1) general relativistic boost factors g have a major impact on the emission because of increasing beaming (e.g. Müller & Camenzind 2004). The radiation is not only shifted in frequency but the observed flux density (F_o) is significantly down-boosted compared to its rest-frame value (F_{rf}) with $F_o = \overline{g^{3-\alpha}} \times F_{rf}$ (Lind & Blandford 1985) for a power law spectrum of energy index α, which is -1.5 for the *XMM-Newton* flare (Porquet et al. 2003). $g^{3-\alpha}$ is to be averaged over an orbit, indicated by the overline, as g varies along the orbit. For $a = 0.994$, and a disk almost viewed edge-on at an inclination angle of $i = 70°$, g varies between 0.064 and 0.834 at $r = r_{ms}$ and $\overline{g^{3-\alpha}} = 0.056$, or the radiation received by the observer is reduced by a factor of ~ 18 compared to its rest frame value. For larger radii the reduction factor approaches unity, but at $r = r_{Rmax} = 2.5$ the radiation is still reduced by a factor of 1.7. The reduction becomes much more pronounced for disks viewed almost face-on. For $i = 15°$ $0.133 \leq g \leq 0.265$ and $\overline{g^{3-\alpha}} < 0.001$. The Lense-Thirring frequency and the Keplerian motion at $r = r_{ms}$ have become unobservable like any other frequency close to the marginal stable orbit. At $r = 2.5$, $\overline{g^{3-\alpha}} < 0.038$. Radiation from the innermost region is on average dimmed by a factor of some hundred, depending on the details of the radial brightness distribution. Because of the large reduction factors the observation of the inner regions of almost face-on accretion disks surrounding supermassive extragalactic black holes in AGN becomes progressively more difficult with increasing a and/or decreasing i. Maybe that this effect contributes to some extent to the faintness of the GC black hole.

Although we have no suggestion which physical process gives rise to the flare we constrain the region from where it comes. Since we see the light modulated with frequencies associated with the marginally stable orbit out to the maximum frequency of the radial epicyclic mode and in between the bulk of the emission arises from a region of $1.37 < r < 2.5$, i.e. the innermost region of the accretion disk.

4. Conclusion

We have discovered five distinct periods in the power density spectrum of the *XMM-Newton* X-ray flare of October 3, 2002. One may wonder about the statistical significance, but these five periods, within their measurement uncertainty, also appear in the power density spectrum of the October 26, 2000 X-ray flare observed by *Chandra*, with perhaps one additional period which, however, does not show up in the *XMM-Newton* flare. Further evidence for the existence of these periods comes from the June 16, 2003 infrared flare (Genzel et al. 2003). The power density spectrum shows a clear increase for at least

two of the periods and possibly for a third period; the remaining two periods were not accessible to the infrared observations. Each of the periods can be identified with one of the four characteristic gravitational modes in accretion disks, i.e. Lense-Thirring precession, Kepler motion, vertical and radial epicyclic oscillation, in such a way that a common value for the black hole mass M_{BH} and the angular momentum a emerges, i.e., $M_{BH} = 2.72^{+0.12}_{-0.19} \times 10^6 \ M_\odot$ and $a = 0.9939^{+0.0026}_{-0.0074}$. The available data on M_{BH} derived from studies of the orbital motion of the S0-2 star and the dark matter concentration in the center of the Milky Way are consistent with our result concerning M_{BH}, which, by the way, is independent of the distance to the black hole. There are indications of a ~ 100 s periodicity in the X-ray data, both in *XMM-Newton* and *Chandra*, but right now, we are reluctant to accept it as firmly established. For further progress in the X-ray domain a flare even brighter than the *XMM-Newton* flare is required, and in the infrared band the temporal resolution should be improved to ~ 10 s. This is particularly important for simultaneous multi-wavelength observations.

References

Baganoff, F. K., Bautz, M. W., Brandt, W. N., et al. 2001, Nature, 413, 45

Baganoff, F. K., Maeda, Y., Morris, M., et al. 2003, ApJ, 591, 891

Baganoff, F. K. 2003, American Astronomical Society, HEAD meeting, 3.02, 35

Genzel, R., Thatte, N., Krabbe, A., Kroker, H., & Tacconi-Garman, L. E. 1996, ApJ, 472, 153

Genzel, R., Schödel, R., Ott, T., et al. 2003, Nature, 425, 934

Ghez, A. M., Duchêne, G., Matthews, K., et al. 2003, ApJ, 586, L127

Lind, K. R., & Blandford, R. D. 1985, ApJ, 295, 358

Liu, S., & Melia, F. 2002, ApJ, 566, L77

Markoff, S., Falcke, H., Yuan, F., et al. 2001, A&A, 379, L13

Melia, F., & Falcke, H. 2001, ARA&A, 39, 309

Merloni, A., Vietri, M., Stella, L., & Bini, D. 1999, MNRAS, 304, 155

Müller, A., & Camenzind, M. 2004, A&A, 413, 861

Muno, M. P., Baganoff, F. K., Bautz, M. W., et al. 2003, ApJ, 589, 225

Nayakshin, S., & Sunyaev, R. 2003, MNRAS, 343, 15

Nowak, M. A., & Lehr, D. E. 1998, in Theory of Black Hole Accretion Discs, ed. M. A. Abramowicz, G. Björnsson, & J. E. Pringle (Cambridge University Press), 233

Orosz, J. A., & Bailyn, C. D. 1997, ApJ, 477, 876

Porquet, D., Predehl, P., Aschenbach, B., et al. 2003, A&A, 407, L17

Remillard, R. A., Morgan, E. H., McClintock, J. E., Bailyn, C. D., & Orosz, J. A. 1999, ApJ, 522, 397

Schödel, R., Ott, T., Genzel, R., et al. 2002, Nature, 419, 694

van der Klis, M. 1989, Timing Neutron Stars, ed. H. Ögelman, & E. P. J. van der Heuvel, NATO ASI Ser., 262, 27

van der Klis, M. 2000, ARA&A, 38, 717

Yuan, F., Quataert, E., & Narayan, R. 2003, ApJ, 598, 301